Mathematical Analysis of Potentiometric Oxygen Sensors for Combustion-Gas Streams

Daniel R. Baker
Mathematics Dept.

Mark W. Verbrugge
Physical Chemistry Dept.

General Motors Research and Development Center, Warren, MI 48090

The mathematical tools necessary to describe quantitatively the chemical processes that dictate the performance of exhaust oxygen sensors are developed. Such sensors are used commonly to monitor exhaust streams generated by internal-combustion processes. Calculated results compare well with available experimental results, although several open questions are identified that require more experimental data. The mathematical formalism for describing the transport of gaseous species through the porous spinel structure protecting the platinum electrode on the exhaust side of the sensor is developed based on the Stefan-Maxwell equations. The kinetic processes occurring at the interface formed by the platinum electrode and the spinel structure, including the oxidation of hydrogen and carbon monoxide and various adsorption-desorption reactions, enter as boundary conditions for the transport equations. The analysis enables one to calculate the sensor's voltage response as a function of the air-to-fuel ratio λ and to investigate phenomena such as the magnitude of the voltage jump in going from rich to lean gas mixtures and the λ value at which this jump occurs.

Introduction

Exhaust-gas-composition sensors are used in feedback-control arrangements in a number of industries that employ internal-combustion processes (Maskell and Steele, 1986; Asad et al., 1992), including the automobile industry, as they allow for control of the intake air-to-fuel (A/F) ratio. The most commonly used exhaust-gas sensor for combustion gas streams involves a measurement of the open-circuit potential generated by the difference in the exhaust-gas composition relative to a reference gas, which is usually air. The potentiometric sensor is referred to as the λ sensor (Dietz et al., 1977), since the exhaust gas composition is a function of the equivalence ratio λ, defined as (Dietz et al., 1977; Verbrugge and Dees, 1993):

$$\lambda = \frac{\text{(mass air/mass fuel)}}{\text{stoichiometric (mass air/mass fuel)}}. \qquad (1)$$

Although the λ sensor cannot be used to determine accurately the extent to which the A/F ratio deviates from stoichiometry, the sensor can be used to determine if the A/F ratio differs from its stoichiometric value and whether there is an excess of air or fuel (Eddy, 1971; Heyne, 1976). It is interesting to note that the relationship between the equivalence ratio and the exhaust gas composition is independent, to good approximation, of the engine's revolutions per minute and other operating conditions. (See, for example, Figure 6 of Sasayama et al., 1991.) A typical plot of the exhaust-gas concentrations considered in this work vs. the equivalence ratio is given in Figure 1 (Logothetis, 1981).

In this article, we provide a steady-state model of the λ sensor. Fleming et al. (1973) note that the typical, commercially available exhaust oxygen sensor (EOS) attains 90% of its steady-state voltage within 50 ms and that the entire automotive feedback control system has a response time ranging from 100 to 200 ms. (See, for example, Figure 9 of Fleming et al., 1973, for a tracing of both vehicle speed and sensor response vs. time.) Similar observations can be found in the works of Young and Bode (1980) and Heyne and den Engelsen (1977). Because

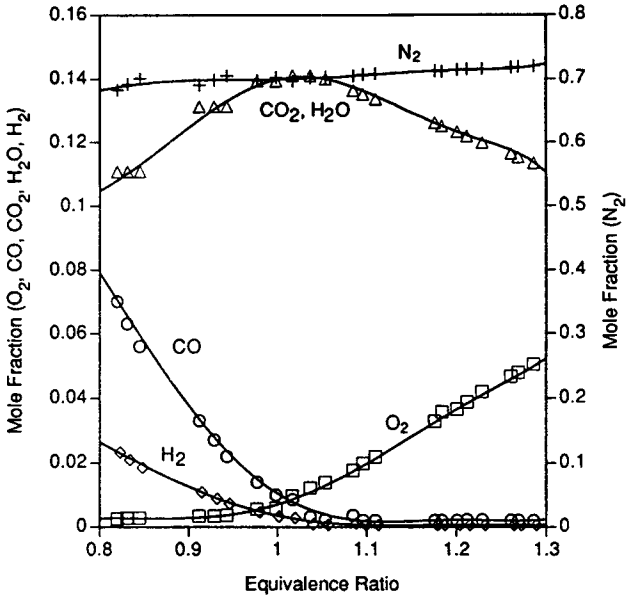

Figure 1. Exhaust-gas mole fractions.

Symbols denote the data provided by Logothetis (1981), and solid curves the fit polynomials of Eq. A10.

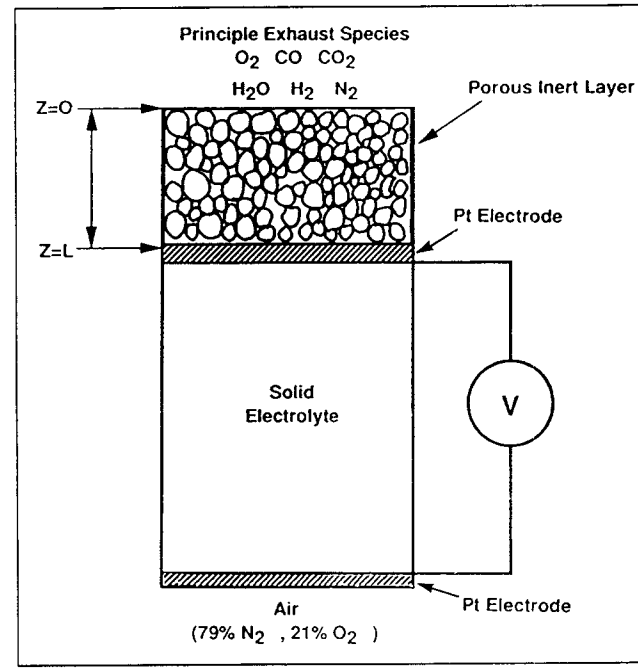

Figure 2. Oxygen sensor.

Boundary conditions addressing interfacial kinetics pertain to the platinum/porous-coating interface, and the Stefan-Maxwell equations address transport through porous coating.

the EOS attains steady-state conditions in such short times, important design considerations can be elucidated by examining steady-state behavior. To simulate higher-frequency cycling behavior of A/F control systems, a transient approach is required. Before undertaking a transient analysis, however, quantifying the steady state seems appropriate.

The λ sensor is shown in Figure 2. The Stefan-Maxwell equations (Hirschfelder et al., 1954; Bird et al., 1960) are used to model the gas transport through the protective, porous spinel layer (Fleming, 1981) that covers the electrode facing the exhaust gases. A variety of possible kinetic processes are investigated for modeling the interface formed by the porous coating and the platinum electrode ($z = L$ in Figure 2). References to its modeling are listed in the article by Anderson and Graves (1981), who themselves provided a model for steady-state oxygen concentration cells. Our model results are compared with the data of Logothetis (1981). We have chosen Logothetis' data for comparison since they are typical of what other researchers have reported and are part of a complete data set in that all of the conditions we need for the modeling work are given in Logothetis' article.

A typical sensor response is shown in Figure 3, as will be discussed in more detail later. Since the objectives of this article revolve around modeling the sensor response, we can use the data in Figure 3 to clarify the questions we would like to address. With regard to the general form of the sensor's potential/equivalence-ratio response as shown in Figure 3, we would like to know:

- What determines the size of the voltage jump in going from rich to lean? (Rich refers to an excess of combustible species relative to oxygen concentration.)
- What determines the λ value at which the voltage switches abruptly? More precisely, why does this switching point take place at a λ value slightly lean of stoichiometry ($\lambda = 1$)?
- What influence will hydrogen-rich fuel supplements, such as methanol, have on the sensor response?
- How are the answers to these questions affected by the sensor's geometry and the exhaust temperature?

The Discussion section summarizes results relevant to these questions obtained by analysis of the proposed model.

Before proceeding with a description of the equations used to formulate the model, we briefly review relevant surface-

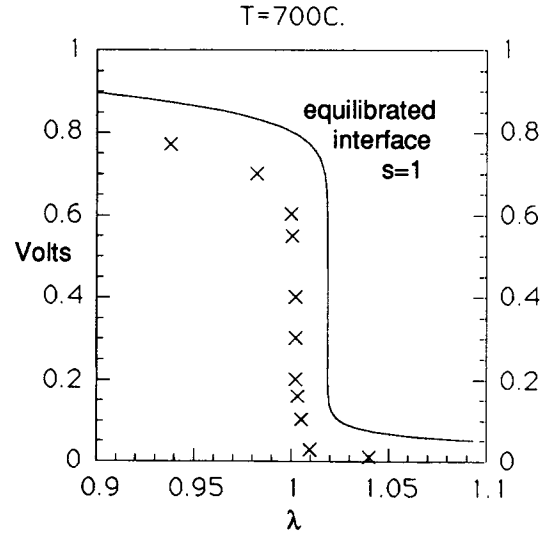

Figure 3. Sensor response.

Sensor voltage for various equivalence ratios: symbols, data from Figure 6 of Logothetis (1981); solid curve, equilibrium calculations with $s = 1$.

chemistry studies and then describe the interfacial chemical reactions considered in this analysis.

Related literature

In spite of the large amount of work devoted to the study of metal/combustible-gas systems, the surface phenomena associated with the prototypical EOS are not well understood over a wide range of pressures and temperatures. For example, we can highlight some of the relatively recent interpretations of the Pt-O_2-CO-CO_2 system (Engel and Ertl, 1979; Berlowitz et al., 1988). Carbon monoxide oxidation on Pt(110) (Bonzel and Ku, 1972a) and polycrystalline platinum ribbon (Pacia et al., 1976) have been explained in terms of the Eley-Rideal mechanism, although the temperature range is critical in determining the operative mechanisms (Bonzel and Ku, 1972b; Berlowitz et al., 1988). In revisiting the Pt(110) system, Bonzel and Burton (1975) favored the Langmuir-Hinshelwood mechanism, in agreement with previous studies (Langmuir, 1921; Palmer and Smith, 1974). The results of Hori and Schmidt (1975) for polycrystalline platinum wire elucidate the problem complexity. For example, Figure 1 of Hori and Schmidt displays the combustion reaction rate (r_{CO_2}) vs. temperature—500 to 1,500 K—for various gas compositions. The reaction-rate curves display multiple maxima and do not lend themselves to simple interpretation. Further complicating kinetic analysis, Matsushima et al. (1977) report two types of chemisorbed oxygen on the basis of Auger electron chemical shifts; the relative concentration of the two distinct surface oxygen species varies with temperature for the polycrystalline platinum foils studied.

While the experimental results obtained for both catalytic and noncatalytic solid-electrolyte sensors correlate with data from the respective metal-gas systems (Haaland, 1980), the precise chemistry of an electrochemical reaction site (ERS) should not be expected to be that of the metal-gas system exclusively. Such an oversimplified interpretation ignores the influence of the solid electrolyte, which contains oxygen-reactant species and electrons and electron holes involved in the electrochemical reactions (Kröger and Vink, 1956; Patterson et al., 1967; Heyne, 1968; Etsell and Flengas, 1970; Wagner, 1975). Determining the chemical environment of the region in which the electrochemical charge-transfer reactions take place continues to be an active area of research (Fouletier et al., 1976; Mizusaki et al., 1987 a,b; Robertson and Michaels, 1990). Knowledge of where the reaction actually takes place is of critical importance with regard to optimizing interfacial and cell performance. Mizusaki et al. (1992) illustrate possible reaction processes at an ERS. In particular, both carbon monoxide oxidation and oxygen reduction can occur through electrochemical reaction along with the chemical oxidation reaction characteristic of metal-gas systems (Anderson and Graves, 1981; Okamoto et al., 1984). Okamato et al. discuss results based on the use of multiple electrochemical reactions to model the Pt-zirconia/O_2-CO-CO_2 system and reference previous studies employing multiple electrochemical reactions. It is difficult to construct experiments that allow one to unambiguously determine if combustible gas species are oxidized by a standard heterogeneous reaction (such as Eq. 5) or by an electrochemical oxidation reaction (such as $CO_{ad} + O^{2-} \rightleftharpoons CO_2 + S + 2e^-$) that is balanced by an electrochemical reduction reaction (Eq. 7) so that the net current is zero for the potentiometric sensor. For this reason, we have chosen to consider only the oxygen reduction electrochemical reaction, in agreement with the approach taken by Anderson and Graves (1981), for example.

Surface chemistry

The chemical reactions taking place on the platinum surface can be divided into three distinct groups: adsorption-desorption reactions, chemical oxidation-reduction reactions, and the electrochemical reaction that generates the voltage response of the electrode. We consider the following three adsorption-desorption reactions:

$$2S + (O_2)_{gas} \rightleftharpoons 2O_{ad}, \tag{2}$$

$$S + (CO)_{gas} \rightleftharpoons CO_{ad}, \tag{3}$$

$$2S + (H_2)_{gas} \rightleftharpoons 2H_{ad}, \tag{4}$$

where S refers to a vacant site on the platinum surface. The adsorbed species are involved in two oxidation reactions:

$$CO_{ad} + O_{ad} \rightleftharpoons CO_2 + 2S, \tag{5}$$

$$2H_{ad} + O_{ad} \rightleftharpoons H_2O + 3S, \tag{6}$$

where the products CO_2 and H_2O diffuse away from the surface and are not involved in any adsorption-desorption processes (Langmuir, 1921; Trapnell, 1955; Laidler, 1965). The electrochemical reaction can be represented as:

$$O_{ad} + 2e^- \rightleftharpoons S + O^{2-} \tag{7}$$

where the superscript -2 is the charge number of the resulting oxygen anions in the zirconia. It follows that the open-circuit potential depends on the concentration of adsorbed oxygen, which in turn depends on the oxygen gas concentration at the surface of the electrode, as well as on the rates of the various reactions listed above. Because the reaction rates are coupled to gas fluxes at the electrode surface, it becomes necessary to consider transport mechanisms when calculating the surface gas concentrations.

In the next section we start by proposing a general model of the transport and kinetic processes that determine the sensor response, based on the chemical reactions stated above. Because of the complicated nature of the chemical processes, the full set of governing equations are capable of describing a wide range of theoretical sensor responses consonant with different values for the physicochemical parameters associated with reactions 2–6. Much of the modeling work was thus reduced to determining what form the sensor response takes for different ranges of parameter values and using this information along with published sensor data to determine if the parameter-value range in question was of practical interest. The complexity of the problem renders a judgement based on exhaustive simulations impractical, and it is thus imperative to find some way of understanding and classifying the model response based on analytic methods. Our analysis is based on an asymptotic expansion of the model equations. This analysis is presented following the derivation of the model and is used in the Results

Table 1. Indices for Six Different Gas Species

Index	Gas Species
1	O_2
2	CO
3	CO_2
4	H_2O
5	H_2
6	N_2

section to formulate hypotheses concerning the state of reactions 2-6. In the Discussion section, we summarize these results and, in particular, address the shift in the voltage jump associated with hydrogen-rich fuel supplements.

Model Equations

Gas transport

The transport model will consider six different gas species, with indices 1 through 6 as shown in Table 1. Let c_i be the concentration of the gas species i, as a function of position, and let x_i be the relative concentration c_i/c (mole fraction), where $c=\Sigma_{i=1}^{6}c_i$. Assuming that both pressure and temperature are constant throughout the gas pores, the ideal gas law implies that the total concentration c will also be a constant. We will be concerned with modeling transport only in the porous spinel layer, and the exhaust-gas phase outside this layer is well mixed with concentrations given as mole fractions x_i^e, determined as a function of the equivalence ratio λ. Because the thickness of the spinel layer is small relative to the dimensions of the sensor, the transport problem will be viewed as one-dimensional, with gas concentrations varying only as a function of the z coordinate in Figure 2. The bulk gas concentrations x_i^e thus provide boundary conditions at $z=0$.

The steady-state material-balance equation for species i takes the form:

$$\nabla \cdot N_i = 0. \tag{8}$$

To complete the description of gas transport, we must give an expression for the flux density N_i, which we provide using the Stefan-Maxwell equations (Hirschfelder et al., 1954; Bird et al., 1960):

$$\nabla x_i = \sum_{j\neq i} \frac{1}{c(D_{i,j}/\tau)} (x_i N_j - x_j N_i). \tag{9}$$

The parameters $D_{i,j}$ are the relative diffusion coefficients for species i in species j. They satisfy the relation $D_{i,j}=D_{j,i}$ and are functions of temperature and pressure. Formulas used in calculating the diffusion coeffficients that are based on kinetic theory and corresponding states arguments are given in Appendix 1. The tortuosity factor τ is used to account for the influence of the porous structure on the transport phenomena (Epstein, 1989). The one-dimensional nature of the problem implies that $N_i=N_{zi}$ for the unknown constant fluxes $N_{z1}, \ldots, N_{z6}$, and

$$x_i' = \sum_{j\neq i} \frac{1}{cD_{i,j}/\tau} (x_i N_{zj} - x_j N_{zi}), \tag{10}$$

where x_i' denotes the derivative of x_i with respect to z. This system is linear in the unknowns x_i, and solutions can be written in the matrix form:

$$X(z) = \exp[zA(N_{zi})] \cdot X(0), \tag{11}$$

where $X(z)$ is the 6-D column vector with entries $x_i(z)$ and the matrix exponential:

$$\exp[zA] = \sum_{i=0}^{\infty} \frac{z^i A^i}{i!}$$

is applied to the 6×6-matrix $A(N_{zi})=[a_{ij}]$, with

$$a_{ii} = \sum_{j\neq i} \frac{N_{zj}}{c(D_{ij}/\tau)}$$

$$a_{ij} = -\frac{N_{zi}}{c(D_{ij}/\tau)} \quad \text{for } i\neq j.$$

To evaluate matrix A, we need to know values for the constants N_{zi}.

The ith entry of the column-vector $X(0)$ is given by the bulk gas concentration x_i^e. The functions $x_i^e(\lambda)$ were fit as polynomials to published data and are given by Eq. A2 in Appendix 1.

All that remains to complete the description of solutions to the transport equations is a way to compute the flux constants N_{zi}, and these are determined by the conditions at the electrode surface. The complete formulation of these conditions depends on the nature of the interfacial kinetic expressions, which are discussed in the next section. For the reactions 2-6, the set of equations:

$$N_{z3} = -N_{z2} \tag{12}$$

$$N_{z4} = -N_{z5} \tag{13}$$

$$N_{z6} = 0 \tag{14}$$

$$N_{z1} = \frac{N_{z2}+N_{z5}}{2} \tag{15}$$

must also hold. The first two of these equations state that the rate at which CO and H_2 are being adsorbed must equal the rate at which CO_2 and H_2O are being produced. The third equation stems from the fact that N_2 is not involved in any of the surface reactions at $z=L$. Under open-circuit conditions, the electrochemical reaction (Eq. 7) is producing no current, so that the rate at which O_2 is adsorbed must equal the rate at which it is being consumed by reaction with CO and H_2, and this is the content of the fourth equation. The four equations (Eqs. 12-15) must be supplemented by two additional equations depending on the interfacial kinetics to solve for the six flux constants N_z; the two additional equations are presented in the next subsection.

We would like to note that a simpler, although less accurate, model of the gas transport can be obtained from Fick's law, instead of the Stefan-Maxwell equations. The analogue to Eq.

11, which gives solutions to the Stefan-Maxwell equations, is then

$$x_i(z) = x_i^e - \frac{zN_{zi}}{c(D_{i,6}/\tau)}. \tag{16}$$

This version of Fick's law becomes exact in the limit as the concentrations of the gas species reacting at the electrode become infinitely dilute in comparison to the concentration of the inert species nitrogen, which, in fact, comprises about 70% of the gas mixture. To understand the errors in this approximation, note that Eq. 10 can be written as:

$$x_i' = -\frac{N_{zi}}{(D_{i6}/\tau)}\left(\sum_{j\neq i}\frac{D_{i6}}{cD_{ij}}x_j\right) + x_i\left(\sum_{j\neq i}\frac{N_{zj}}{c(D_{ij}/\tau)}\right).$$

If

$$\sum_{j\neq i}\frac{D_{i6}}{D_{ij}}x_j \approx 1 \quad \text{and} \quad x_i \approx 0,$$

then Fick's law will hold with D_{i6} as the diffusion coefficient for the ith species. The concentrations of N_2, CO_2, and H_2O comprise about 95% of the gas mixture. Because the fluxes of these species are coupled via Eqs. 12–15 to the fluxes of the remaining more dilute species, they remain small and their relative concentrations remain fairly constant. In some test comparisons, it was found that the difference in calculated voltages using Fick's law as opposed to the Stefan-Maxwell equations was less than 1%, except near the voltage jump going from rich to lean, where the differences can become much larger. It should be noted that for the conditions of this study, Fick's law will not preserve constant pressure throughout the gas.

Interfacial kinetics

We turn now to the derivation of boundary conditions at the electrode surface under various assumptions about the chemical reactions (Eqs. 2–6). We consider first the most general situation in which none of the reactions are in equilibrium and then make equilibrium assumptions at various points to simplify these equations.

The usual starting point for describing interfacial chemical kinetics begins with a reaction-rate expression for reaction ℓ of the form (Laidler, 1965):

$$r_\ell = k_{f,\ell}\prod_i (c_i^{\nu_{i,\ell}})_{\text{Reactants}} - k_{b,\ell}\prod_i (c_i^{\nu_{i,\ell}})_{\text{Products}},$$

where k_f and k_b are the forward and backward rate constants and the stoichiometric coefficient of the reactant or product species i for reaction ℓ is given by $\nu_{i,\ell}$. The symbol c_i is employed as a generic concentration, which for gaseous species will be given as mole fractions (x_i, $i=1, \ldots, 6$) and for surface-adsorbed species will be given in terms of fractional surface coverage (θ_i, $i=1$, 2, 5, and v). The fractional coverage of vacant sites, θ_v, is discussed below. Note, however, that from the definition of fractional coverage one has:

$$\theta_1 + \theta_2 + \theta_5 + \theta_v = 1. \tag{17}$$

The flux of gaseous species i to the platinum surface is related to the reaction rate expressions by:

$$N_{zi} = \sum_\ell [(\nu_{i,\ell})_{\text{Reactants}} - (\nu_{i,\ell})_{\text{Products}}]r_\ell.$$

Using this formalism, we can now construct our boundary conditions for the gas-transport problem.

The general form of these boundary conditions is given in Appendix 4; we will give a simplified form here, based on the assumption that the fractional coverage θ_v of vacant sites is constant and does not depend on the equivalence ratio λ. We expect this to be valid on the rich side of the switching point, as the platinum surface should be relatively clean (devoid of adsorbed species) for the temperatures of interest (Haaland, 1980). For example, when the carbon monoxide concentration is greater than that of oxygen, the oxygen concentration on the platinum surface should be kept low due to the oxidation of carbon monoxide, and the carbon monoxide fractional coverage should remain low (relative to that of the vacant sites) for surface temperatures above 300°C (Bonzel and Ku, 1972a; Matsushima et al., 1977). Under such conditions, θ_v should be close to one and thus relatively constant. Such ideal behavior may not always be observed in practice (Hori and Schmidt, 1975). On the lean side of the switching point, it seems possible that variations in θ_v could arise, since the fraction of sites occupied by adsorbed oxygen may exceed the fraction of vacant sites (Langmuir, 1921; Matsushima et al., 1977). These variations could influence the voltage response of a sensor to some degree. (As one approaches the lean-side plateau, however, these effects die out, because the oxidation reaction rates become negligible.) It is shown in Appendix 4 that variations in θ_v can be included in the model, but necessitate introducing additional parameters, containing unknown adsorption-desorption rate-constant ratios, to the model equations. The ability of the model that assumes constant θ_v to explain available data will help evaluate the constant-vacancy-concentration assumption.

Using our reaction-rate and flux expressions (with the assumption of constant θ_v), we can write our boundary conditions as:

$$N_{z1} = k_{f,1}x_1 - k_{b,1}\theta_1^2 \tag{18}$$

$$N_{z2} = k_{f,2}x_2 - k_{b,2}\theta_2 \tag{19}$$

$$N_{z5} = k_{f,5}x_5 - k_{b,5}\theta_5^2, \tag{20}$$

where the mole fractions x_i are taken at the electrode surface, at $z=L$. Fluxes for the CO_2 and H_2O species are determined by the oxidation reactions:

$$N_{z3} = k_{f,3}x_3 - k_{b,3}\theta_2\theta_1 \tag{21}$$

$$N_{z4} = k_{f,4}x_4 - k_{b,4}\theta_5^2\theta_1. \tag{22}$$

Case 1: Equilibrated Interface. Consider now the equilibrium situation in which all of the rate constants are so large that the lefthand sides of Eqs. 18–22 can be set to zero, and the fluxes drop out of these equations. Equations 18–20 can be solved for θ_1, θ_2, and θ_5, and these expressions can be inserted into Eqs. 21–22 yielding

$$\frac{x_3}{x_2\sqrt{x_1}} = K_I\sqrt{p} \tag{23}$$

$$\frac{x_4}{x_5\sqrt{x_1}} = K_{II}\sqrt{p}, \tag{24}$$

where p is pressure, and the quantities $K_i\sqrt{p}$ (i = I or II) replace the appropriate ratios of backward forward rate constants. The equilibrium constants K_i are related to tabulated equilibrium constants for the oxidation reactions by a scale factor, $K_i = s_i\tilde{K}_i$, where $\tilde{K}_i$ are tabulated equilibrium constants for the oxidation reactions. For numerical purposes, the following fit expressions were used to represent the tabulated equilibrium constants (Smith and Van Ness, 1975):

$$\tilde{K}_I = 3.72\times 10^{-5}\exp\left(\frac{33{,}800}{T}\right) \quad \text{and}$$

$$\tilde{K}_{II} = 9.78\times 10^{-4}\exp\left(\frac{30{,}200}{T}\right).$$

The units on $\tilde{K}_I$ and $\tilde{K}_{II}$ are atm$^{-1/2}$. A physical interpretation of the parameters s_i is given in the Results section.

Case 2: Hindered Hydrogen Adsorption-Desorption. We turn now to the modification of Eqs. 23 and 24 that arises when the equilibrium assumption is dropped for the hydrogen adsorption-desorption reaction (Eq. 4). The motivation for choosing the hydrogen adsorption-desorption reaction, relative to the oxygen or carbon monoxide adsorption-desorption reactions, is discussed in the Results section. In this case, Eq. 20 must be used in unsimplified form to solve for θ_5:

$$\theta_5^2 = \frac{k_{f,5}}{k_{b,5}}\left(-\frac{N_{z5}}{k_{f,5}} + x_5\right). \tag{25}$$

Since the righthand side of this differs from the equilibrium expression only in the addition of the term $-N_{z5}/k_{f,5}$, it suffices to replace x_5 with $x_5 - N_{z5}/k_{f,5}$ in Eq. 24:

$$\frac{x_4}{(x_5 - N_{z5}/k_{f,5})\sqrt{x_1}} = K_{II}\sqrt{p}. \tag{26}$$

Equation 23 still remains valid in its original form in this situation.

Case 3: Equilibrium Adsorption-Desorption, Hindered Oxidation. For the last case we consider, suppose that all adsorption-desorption reactions are in equilibrium, but drop the equilibrium assumption for the two oxidation reactions (Eqs. 5 and 6). In this case, one must use Eqs. 21 and 22 in unsimplified form, but one can use the equilibrium forms of Eqs. 18–20 to solve for the surface concentrations θ_1, θ_2, and θ_5. After substituting the results into Eqs. 21 and 22, and comparing these equations with the equilibrium forms (Eqs. 23 and 24), we obtain:

$$N_{z3} = k_3\left(-x_2\sqrt{x_1} + \frac{x_3}{K_I\sqrt{p}}\right) \tag{27}$$

$$N_{z4} = k_4\left(-x_5\sqrt{x_1} + \frac{x_4}{K_{II}\sqrt{p}}\right), \tag{28}$$

where the rate constants k_3 and k_4 have been introduced. Equations 27 and 28 tend to their equilibrium form given by Eqs. 23 and 24, as k_3 and k_4 tend to ∞.

Sensor voltage response

Equations 12–15, together with Eqs. 23 and 24 for case 1 (the equilibrated interface), Eqs. 23 and 26 for case 2 (hindered hydrogen adsorption-desorption), or Eqs. 27 and 28 for case 3 (equilibrium adsorption-desorption, hindered oxidation), make a total of six equations that can be used to solve for the flux-density constants $N_{z1}, \ldots, N_{z6}$. Note that the variables x_i at $z = L$ (the electrode surface) must be evaluated using formula 11, so that they too are functions of N_{zi}.

Once the system of equations has been solved, the open-circuit potential can be calculated using (Dietz et al., 1977; Maskell and Steele, 1986; Asad et al., 1992)

$$V = -\frac{RT}{4F}\ln\left[\frac{x_1(L)p}{p_{1,\text{ref}}}\right]. \tag{29}$$

The exhaust-gas pressure, p, is set to 1.1 atm, and the air-reference partial pressure of oxygen, $p_{1,\text{ref}}$, is taken to be 0.21 atm. The use of Eq. 29 is consistent with equilibrated oxygen adsorption-desorption (compare Eq. 7), in agreement with cases 1, 2 and 3. The sign convention used in Eq. 29 was chosen to yield positive voltages for the conditions of this work and reflects common practice in the oxygen sensor literature.

Note that for the equilibrated interface (case 1), the above system of equations for calculating V does not in any way depend on the thickness L of the porous layer being modeled. (This fact follows from the dimensionless form of the equations in the next section.) In fact, a much stronger statement holds: under the equilibrium assumption for all reactions, the above analysis is valid for multidimensional porous-layer geometries of arbitrary size and shape, as long as the bulk gas concentrations at the surface of the layer are constant, and this should be the case if the exhaust gas outside the porous layer is well mixed. The equilibrium model thus predicts that the steady-state behavior of such sensors should not depend on the thickness of the porous covering material, its tortuosity factor τ, or the shape of the sensor it covers, although these factors can certainly influence the transient behavior and thus the frequency response of the sensor. The proof of these statements follows by reducing the analogous multidimensional calculations to the same one-dimensional problem that has already been described, and this can be done using methods developed in a previous article (Baker, 1993). It should be emphasized, however, that the voltage response does depend on the geometry of the sensor, and its porous layer, if any of the reactions at the electrode surface are kinetically hindered.

Perturbation analysis of the equation system

The dimensionless constants $K_I\sqrt{p}$ and $K_{II}\sqrt{p}$ are large numbers; for example, typical values at 700°C will be on the order of 10^{10}. These large values are responsible for the sudden voltage jump when going from rich to lean equivalence ratios and

make the calculation of the open-circuit potential a difficult numerical task. Some of these difficulties can be indicated by the following considerations: The size of $K_I\sqrt{p}$ and $K_{II}\sqrt{p}$ forces the concentrations of CO and H_2 at the electrode surface to be very small in the lean range, whereas the concentration of O_2 becomes very small in the rich range. As a result, to obtain sufficient accuracy in the calculations, one is forced to use different calculation procedures in each of these two regimes. In principle, one should change calculation procedures as one moves through the switching point where the voltage jump occurs, but the location of this switching point is not known ahead of time.

On the other hand, the size of the constants $K_I\sqrt{p}$ and $K_{II}\sqrt{p}$ suggests the possibility of an asymptotic analysis, and this is what we have done. Specifically, we will present a perturbation analysis in the small parameter $\epsilon = 1/(K_I\sqrt{p})$. In most operating regimes, at 700°C, for instance, ϵ is so small that the errors associated with the leading order term in this analysis are also negligibly small. (These errors will be discussed later.) The analysis will also allow us to compute where the voltage jump occurs as a separate calculation, resolving the difficulty mentioned above. In addition, the perturbation analysis provides some general insight into how the voltage response of the sensor depends on various electrode boundary conditions discussed in the last section, so that some of these possibilities can be excluded as physically unrealistic.

We nondimensionalize the model equations using the following definitions:

$$\tilde{N}_{zi} = \frac{L\tau}{cD} N_{zi} \quad \tilde{D}_{ij} = \frac{D_{ij}}{D} \tag{30}$$

$$\epsilon = \frac{1}{K_I\sqrt{p}} \quad \tilde{z} = \frac{z}{L} \tag{31}$$

$$\tilde{K} = \frac{K_I}{K_{II}} \quad \alpha_H = \frac{L\tau k_{f,5}}{cD} \tag{32}$$

$$\tilde{k}_i = \frac{L\tau k_i}{cD} \quad \text{for} \quad i = 3, 4. \tag{33}$$

All differentiation of dimensionless quantities will be understood to be taken with respect to the scaled coordinate $\tilde{z}$. The quantity D should be chosen to eliminate temperature dependence to the greatest extent possible in the diffusion coefficients. As the formulas in Appendix 1 show, the ratios of coefficients D_{ij}, for $i, j \neq 4$, are temperature-independent, a fact which will be useful later on, and we have set $D = D_{56}$.

The dimensionless form of the Stefan-Maxwell equations is the same as its dimensioned form (Eq. 10), except that constants c and τ have been removed and the solutions to the Stefan-Maxwell equations in dimensionless form will still be given by Eq. 11, again with constants c and τ removed from matrix A. Similar statements also hold for Fick's law. The flux equations (Eqs. 12–15) remain unchanged, except for the fact that all fluxes in the equations now appear in dimensionless form.

We will consider each of the three sets of boundary conditions given in the last section. The full analysis will first be done for the equilibrated interface, and then the necessary changes indicated for the other two sets of conditions.

Case 1: Equilibrated Interface. The equilibrium boundary conditions (Eqs. 23 and 24) now can be written as:

$$\epsilon x_3 = x_2\sqrt{x_1} \tag{34}$$

$$\epsilon\tilde{K}x_4 = x_5\sqrt{x_1}, \tag{35}$$

at $\tilde{z} = 1$. We postulate then that:

$$\tilde{N}_{zi} = \tilde{N}_{zi,0} + \epsilon\tilde{N}_{zi,1} + \ldots \tag{36}$$

$$x_i = x_{i,0} + \epsilon x_{i,1} + \ldots, \tag{37}$$

where the terms not written are assumed to be at least of order ϵ^2. We turn now to the problem of calculating the leading order terms in the expression for $x_1(1)$ which will then be used to calculate the voltage V via Eq. 29. This leading order term approximates the exact voltage for small values of ϵ quite accurately.

When $\epsilon = 0$, Eq. 34 takes the form:

$$x_{2,0}(1)\sqrt{x_{1,0}(1)} = 0, \tag{38}$$

which implies that either $x_{1,0}(1)$ or $x_{2,0}(1)$ must equal zero. Intuitively, one expects $x_{1,0}(1)$ to vanish in the rich fuel regime, whereas $x_{2,0}(1)$ will vanish in the lean fuel regime. We examine each of these two cases separately.

Suppose first that $x_{2,0}(1) = 0$. The leading-order equations that now replace Eqs. 34 and 35 are:

$$\begin{aligned} x_{2,0}(1) &= 0 \\ x_{3,0}(1)x_{5,0}(1) &= 0. \end{aligned} \tag{39}$$

In these two equations, Eq. 11 is to be used to determine $x_{i,0}$ as functions of $\tilde{N}_{zi,0}$, so that the resulting six equations can now be used to determine six unknowns $\tilde{N}_{zi,0}$. Once this has been done, $x_{1,0}(1)$ follows from Eq. 11 and can be used to determine voltage V from Eq. 29.

Consider now the second alternative for solving Eq. 38: $x_{1,0}(1) = 0$. One can then use this equation to replace Eq. 39, and from Eqs. 34 and 35 one finds that:

$$\tilde{K}x_{4,0}(1)x_{2,0}(1) = x_{3,0}(1)x_{5,0}(1). \tag{40}$$

These two equations, along with Eqs. 12–15, allow one to determine the values for $\tilde{N}_{zi,0}$ and $x_{i,0}(1)$. Equation 34 now implies that $x_{1,1}(1) = 0$ and

$$x_{1,2}(1) = \left[\frac{x_{3,0}(1)}{x_{2,0}(1)}\right]^2.$$

The leading order expression $x_{1,0}(1)$ (on the lean side) or $\epsilon^2 x_{1,2}(1)$ (on the rich side) can now be inserted into Eq. 29 to compute the voltage:

$$V = \begin{cases} \dfrac{RT}{4F}\ln\dfrac{x_{1,0}(1)p}{p_{1,\text{ref}}}, & \text{if } x_{2,0}(1) = 0, \\ \dfrac{RT}{4F}\left[2\ln(\epsilon) + 2\ln\dfrac{x_{3,0}(1)}{x_{2,0}(1)} + \ln\dfrac{p}{p_{1,\text{ref}}}\right], & \text{if } x_{1,0}(1) = 0. \end{cases}$$

If one tries to plot voltage as a function of equivalence ratio λ, one will find that the first formula for V holds in the lean fuel range and the second formula holds in the rich fuel range. At some value λ_0 for the equivalence ratio, the voltage will jump as one switches from one solution branch to the other. This is what causes the "binary response" of the open-circuit sensor. The change in solution branches becomes necessary when one branch starts to produce negative values for either $x_{1,0}(1)$ or $x_{2,0}(1)$.

Note that the value of λ_0 can be found by solving the two equations:

$$x_{1,0}(1) = x_{2,0}(1) = 0, \tag{41}$$

in addition to the four flux equations (Eqs. 12–15) and Eq. 40. This makes a total of seven equations, allowing one to determine λ_0 as well as the values $\tilde{N}_{z1,0}, \ldots, \tilde{N}_{z6,0}$ associated with it. What makes the open-circuit sensors useful is the fact that this switching usually takes place at or near stoichiometry, and an analytic formula for predicting the switching point is desirable. While it is possible to determine this point by numerically solving the equations associated to the Stefan-Maxwell transport law, the complicated nature of Eq. 11 makes it difficult to extract any useful analytic information. The situation is different, however, if Fick's law is used to model the gas transport; in this case, Eqs. 41 and 40 in conjunction with Fick's law imply that:

$$\tilde{N}_{zi,0} = \tilde{D}_{i6} x_i^e, \tag{42}$$

for $i = 1, 2, 5$. The equation

$$\tilde{D}_{16} x_1^e(\lambda_0) = \frac{\tilde{D}_{26} x_2^e(\lambda_0) + \tilde{D}_{56} x_5^e(\lambda_0)}{2} \tag{43}$$

now follows from Eq. 15. The derivation of this equation is similar to that used by Brailsford and Logothetis (1985) to calculate the switching point of a TiO_2 oxygen sensor, although the details of the two calculations are different. Recall that functions $x_i^e(\lambda)$ are known inputs to the model (Appendix 1), so that these functions can be inserted into Eq. 43 to solve for λ_0. Note that if all diffusion coefficients in Eq. 43 were equal, the switching would occur exactly at stoichiometry. We underscore, however, that the derivation of Eq. 43 is based on a Fick's law approximation to transport, which also contains a certain amount of inaccuracy. Note also that the dimensionless diffusion coefficients appearing in Eq. 43 are temperature-independent, so that this formula predicts that, under equilibrium conditions for all reactions, the switching point should also be temperature-independent.

In the Results section, we shall apply formula 43 to data where either CO or H_2 is present, but not both. In this situation, we note that the equivalence ratio λ can be computed as:

$$\lambda = \frac{x_1^e / x_i^e}{(x_1^e / x_i^e)_{\text{stoichiometry}}},$$

where x_i^e refers to the reacting species CO or H_2.

Case 2: Hindered Hydrogen Adsorption-Desorption. The dimensionless version of Eq. 26 is:

$$\epsilon \tilde{K} x_4 = \left(x_5 - \frac{\tilde{N}_{z5}}{\alpha_H} \right) \sqrt{x_1}, \tag{44}$$

at $\tilde{z} = 1$. The analysis now proceeds as in case 1, and we omit the details. The equation for the switching point obtained from Fick's law (analogous to Eq. 43) now has the form:

$$\tilde{D}_{16} x_1^e(\lambda_0) = \frac{1}{2} \left[\tilde{D}_{26} x_2^e(\lambda_0) + \frac{\tilde{D}_{56} x_5^e(\lambda_0)}{1 + \tilde{D}_{56}/\alpha_H} \right] \tag{45}$$

Case 3: Equilibrium Adsorption-Desorption, Hindered Oxidation. The dimensionless versions of Eqs. 27 and 28 are:

$$\tilde{N}_{z3} = \tilde{k}_3 (- x_2 \sqrt{x_1} + \epsilon x_3) \tag{46}$$

$$\tilde{N}_{z4} = \tilde{k}_4 (- x_5 \sqrt{x_1} + \epsilon K x_4). \tag{47}$$

The behavior of the voltage-λ curves obtained from these equations depends on the size of parameters $\tilde{k}_3$ and $\tilde{k}_4$. The analysis is given in Appendix 2.

Accuracy of the Perturbation Solution. If the formal assumptions we have been making hold, the errors in our voltage estimates should be order ϵ, but this analysis does not take into account the size of the coefficients appearing in the ϵ series. The problem can be seen from the perturbation analysis of Eq. 34, which yields:

$$x_{3,0}(1) = \begin{cases} x_{2,0}(1)\sqrt{x_{1,2}(1)} & \text{if} \quad x_{1,0}(1) = 0 \\ x_{2,1}(1)\sqrt{x_{1,0}(1)} & \text{if} \quad x_{2,0}(1) = 0. \end{cases} \tag{48}$$

If $x_{3,0}(1)$ is nonzero but both $x_{1,0}(1)$ and $x_{2,0}(1)$ vanish, these equations have no solutions for the higher-order terms. We are thus forced to conclude that near the switching point between the two leading order solutions, where Eq. 48 becomes singular, the analysis becomes invalid. To approximate accurately solutions in this region, it becomes necessary to choose another form for the dependence of the variables on ϵ and perform a singular perturbation analysis, as shown in Appendix 3. The calculations discussed there indicate, however, that the above analysis only starts to become invalid for values of λ very close to the critical value λ_0 at which the voltage jump takes place. Figure 4 compares the two different perturbation expansions at values near the switching point. The results indicate good agreement between the two expansions when $|\lambda - \lambda_0| > 20\epsilon^{2/3}$, and we note again that at 700°C the value of ϵ is about 10^{-10}.

Results

The simplest model to consider corresponds to an equilibrated interface with the activity of the adsorbed species equal that of the corresponding gas-phase species immediately adjacent to the surface (case 1, $s = 1$). The required diffusion coefficients and the equilibrium constants can be taken from standard literature sources, and the thickness and tortuosity of the spinel coating do not affect the steady-state sensor voltage. This condition is compared with the experimental data of Logothetis (1981) in Figure 3, which shows two important differences between the data and case 1 with $s = 1$. First, the voltages on the rich side (the rich-side plateau) are too high.

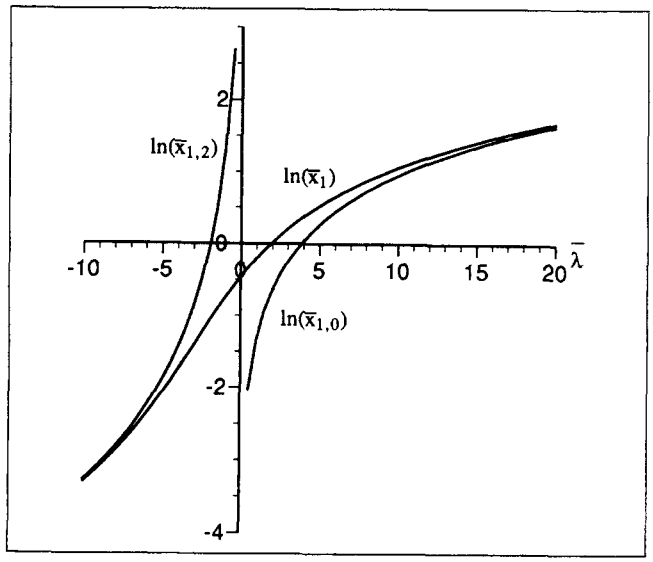

Figure 4. Comparison of the two different perturbation expansions near the switching point.

Leading-order expressions for $\ln[\bar{x}_1(1)]$ as a function of $\bar{\lambda} = \epsilon^{-2/3}(\lambda - \lambda_0)$: on the rich side, good agreement is observed for $\bar{\lambda} < -10$; on the lean side the two approximations agree well for $\bar{\lambda} > 20$. The quantities are all in dimensionless form.

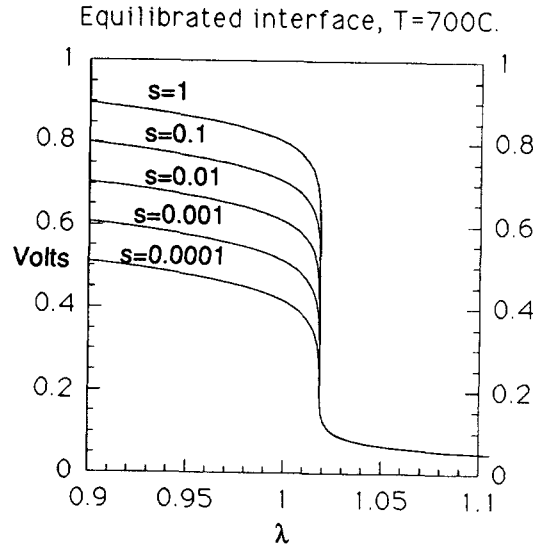

Figure 5. Altering the rich-side sensor response.

Calculated equilibrium sensor response for various values of the parameter $s_I = s_{II} = s$.

[We shall not address the poor fit in the lean range other than noting that the lean plateau is very insensitive to the values of s and α_H (Figures 5 and 7) and that available literature data usually show sensor voltages more in agreement with our calculations. For example, the experimental data in Figure 10 of Heyne (1976) for a sensor in an actual automobile exhaust-gas environment shows a 50-mV sensor voltage for $\lambda = 1.1$, in agreement with our lean-side calculations.] Second, the equivalence ratio at which the voltage switches abruptly from values characteristic of rich gas streams to that of lean gas streams, which we refer to as the switching point λ_0, occurs too far into the lean regime.

The sensor voltage can be reduced in the rich range by considering relevant adsorption-desorption equilibria, which leads to the introduction of the parameters s_I and s_{II}. If we define equilibrium constants for reactions 2 and 3 as:

$$K_O = \frac{\theta_I^2}{\theta_v^2 x_1 p} \quad \text{and} \quad K_{CO} = \frac{\theta_2}{\theta_v x_2 p},$$

then we can write

$$\tilde{K}_I = \frac{\theta_v^2 x_3 p}{\theta_I \theta_2}$$

$$= \frac{1}{K_{CO}\sqrt{K_O}} \frac{x_3}{x_2\sqrt{x_1 p}}$$

or

$$K_I = \frac{x_3}{x_2\sqrt{x_1 p}}$$

$$= s_I \tilde{K}_I$$

where $s_I = K_{CO}\sqrt{K_O}$. A similar analysis for the hydrogen oxidation reaction leads to $s_{II} = K_H\sqrt{K_O}$, where $K_H = \theta_S^2/\theta_v^2 x_S p$. If $K_{CO} = K_H$, then $s_I = s_{II}$. For this work, we shall assume $K_H = K_{CO}$, leading to $s = s_I = s_{II}$. The influence of the parameter s on the sensor voltage is shown in Figure 5. Interfaces characterized by a low s value maintain lower surface concentrations of adsorbed species, which ultimately participate in the oxidation reactions. Thus, surfaces that are characterized by a low value of s might be viewed from an overall perspective as less catalytic to CO and H_2 oxidation.

It is also possible to depress the rich-side plateau by introducing kinetic resistance to both of the oxidation reactions described by Eqs. 5 and 6. The asymptotic analysis for the boundary conditions in this case is given in Appendix 2, where it is shown that if the oxidations reactions are not equilibrated, then the voltage corresponding to the rich-side plateau depends on the spinel-coating thickness. We are not aware of literature data that indicate such a dependence on the coating thickness; hence, we have instead opted to employ the use of equilibrated oxidation reactions consonant with the discussion of Figure 5 to describe the rich-side plateau.

We now address the switching point λ_0. The first observation to be made is that λ_0 has no dependence on the value of s, or more generally the size of ϵ (assuming that ϵ remains small). To alter the calculated value of λ_0, one must thus abandon the equilibrium assumptions set forth in case 1 and include some form of kinetic resistance, as appears either in the oxidation reactions (Eqs. 21 and 22) or in the adsorption-desorption reactions (Eqs. 18–20). Rather than introducing these assumptions in their most general form, we now present arguments which allow us to include these effects in the form given in case 2.

We start by addressing the question of whether or not kinetic hindrance in the oxidation reactions can be used to move the switching point, and we will conclude that it cannot. This entails an analysis of the boundary conditions in case 3, as given in Appendix 2, and the results of the hindered oxidation analysis are given in Figure 6. In addition to the rich and lean

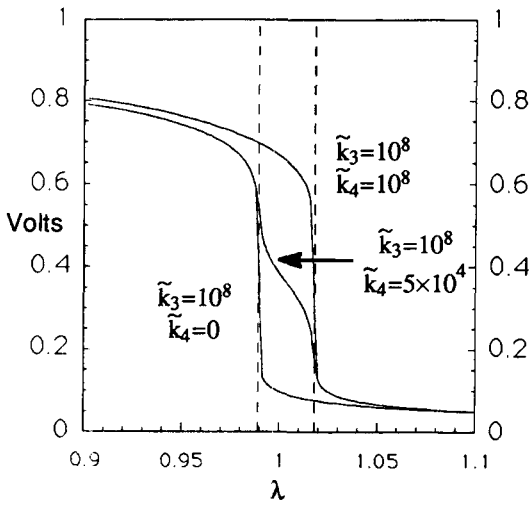

Figure 6. Effect of hindered oxidation reactions.

When $\tilde{k}_3=\tilde{k}_4$ are large, there is only one switching point, at the same place it occurs under the assumption of an equilibrated interface for all reactions. When $\tilde{k}_3$ is large but $\tilde{k}_4=0$, there is again only one switching point, but it moves to where it would be if the hydrogen reaction were turned off. When $\tilde{k}_3 \gg \tilde{k}_4 \gg 1$, both switching points occur in the same curve.

plateaus, the hindered oxidation introduces another region centered about stoichiometry. This is shown by the middle curve in Figure 6, for which $\tilde{k}_3 \gg \tilde{k}_4 \gg 1$: the H_2-oxidation is much more hindered than the CO oxidation. Considering the sensor's behavior as the gas composition is changed from rich values on the left of Figure 6 to leaner values in the middle region, the CO concentration at the electrode surface drops first, so that in the middle region it is much smaller than the H_2 concentration. At the leanest λ values on the right of Figure 6, both concentrations have dropped to very small values. It is important to note that changing the values of $\tilde{k}_3$ and $\tilde{k}_4$ will change the concentrations in each of the three regions, but it has no effect on the placement of the two switching points. The left-most switching point occurs at the same place, if the CO reaction is in equilibrium and the hydrogen-reaction is completely hindered. The right-most switching point occurs at the same place when all reactions are in equilibrium (case 1). The left-most curve shows that as the hydrogen reaction becomes completely hindered, the surface concentrations in the middle region are indistinguishable from those in the lean region, so that only the left-most switching point is discernible. On the other hand, the right-most curve shows that if the H_2 oxidation is no more hindered than the CO oxidation, the surface concentrations in the middle region are indistinguishable from those in the rich region, and only the right-most switching point is discernible. We are unaware of any experimental evidence for the existence of two switching points in voltage-response curves, and we have rejected the use of hindered oxidation reactions for this reason. As noted in the discussion of the rich-side voltages, however, if both the H_2 oxidation and the CO oxidation are hindered equally (the right-most curve), varying the resulting single rate-constant value does not change the switching point, but does vary the rich-side plateau in a fashion that depends on the porous-layer geometry, as it appears in the dimensionless groups $\tilde{k}_3$ and $\tilde{k}_4$.

We are thus led to focus on the adsorption-desorption reactions, and there are three such reactions (Eqs. 18-20) in which kinetic hindrance can occur. We focus first on the adsorption-desorption of CO and O_2. Figure 10 of Logothetis (1981) compares data from a simulated exhaust gas consisting exclusively of carbon monoxide, oxygen and nitrogen. It also shows that at 500°C, the data compare well with equilibrium calculations. This data comparison motivates our assumption that the adsorption-desorption of CO and O_2 is in equilibrium. Note in particular that the switching point for the data occurs very close to stoichiometry. This is consistent with formula 43 for the switching point, given in the last section, considering the the diffusion coefficients $\tilde{D}_{16}$ and $\tilde{D}_{26}$ are close to equal. Similar data sets are also given in Figure 6 of Anderson and Graves (1981), which allow the comparison of the simulated mixtures O_2-CO-N_2 and O_2-H_2-N_2 at 600°C. Again, the switching point for the O_2-CO-N_2 mixture occurs close to stoichiometry, but the situation differs for the O_2-H_2-N_2 mixture. Applying formula 43 to the latter mixture and noting that the ratio of $\tilde{D}_{16}$ to $\tilde{D}_{56}$ is close to 1/4, one expects the switching point to occur near $\lambda=4$ if equilibrium conditions hold. Instead, the data indicate a switching point somewhat greater than $\lambda=2$. We infer from this that the hydrogen adsorption-desorption is not in equilibrium. The switching point would be consistent with the modified formula 45 given under the assumptions of case 2. It thus seems reasonable to assume that hydrogen species arriving at the platinum surface adsorb dissociatively in a rather slow process relative to that of carbon monoxide and oxygen. The hindered adsorption-desorption of hydrogen, relative to carbon monoxide and oxygen, may be rationalized in part by the stronger binding of carbon monoxide and oxygen to platinum surfaces seen at lower temperatures (Langmuir, 1921; Trapnell, 1955; Laidler, 1965; Engel and Ertl, 1979). Consequently, we have chosen to introduce kinetic limitations in our description of the hydrogen adsorption-desorption process and assume the oxygen and carbon monoxide adsorption-desorption processes are in equilibrium. We note, however, that the treatment of the adsorption-desorption reactions for the H_2-CO-O_2-N_2 system has remained an active area of research before and since Langmuir's (1921) work on this system. As suggested by Haaland (1980), it may be that platinum/zirconia/platinum geometries can be used to answer some of the fundamental questions regarding the chemical processes associated with the H_2-CO-O_2-N_2 system. More experimental data would help quantify the phenomena governing the sensor response. For example, as suggested above and as will be noted below, data collected with different porous coating thicknesses could remove some of the open questions.

It is important to note that although the equilibrium treatment provided for the rich-side plateau lacked any dependence on the porous coating thickness, the switching point treatment we have offered, which gives rise to the dimensionless group α_H, does depend on the coating thickness. At this time, a consistent data set showing the dependence of the switching point on the coating thickness is unavailable. It should, however, be possible to conduct experiments to investigate the effect of the coating thickness on the switching point.

The influence of α_H on the sensor's potential response is shown in Figure 7. For $\alpha_H=\infty$, the equilibrium description for the sensor response is recovered, and the switching point λ_0 is greater than that of Logothetis' data. The other extreme

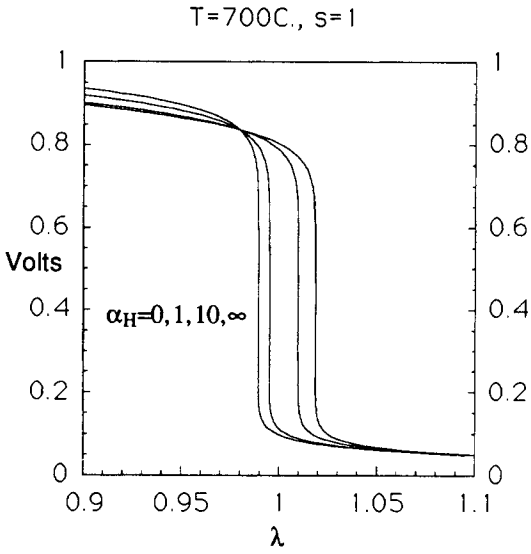

Figure 7. Altering the switching point.

Calculated sensor response for various values of the parameter α_H: $\alpha_H = 0$, no hydrogen adsorption-desorption reaction and $N_{\ddot{s}5} = 0$; $\alpha_H = \infty$, equilibrated hydrogen adsorption-desorption reaction (equilibrium curve of Figure 3).

represents the situation in which hydrogen is so hindered kinetically that the gaseous hydrogen flux at the surface (and therefore throughout the porous coating thickness) may be taken to be zero, and λ_0 is too small relative to the data of Logothetis. By varying the value of α_H we can translate between the two extremes and match the experimental data for the switching point.

The final fit values of the parameters s and α_H are given in Figure 8, along with the associated theoretical sensor response and the data of Logothetis. The fit is quite good with the exception of the lean plateau, which, as noted earlier, may be attributed to experimental problems.

The surface mole fractions of the various species, relative to their respective values in the exhaust-gas stream, are shown

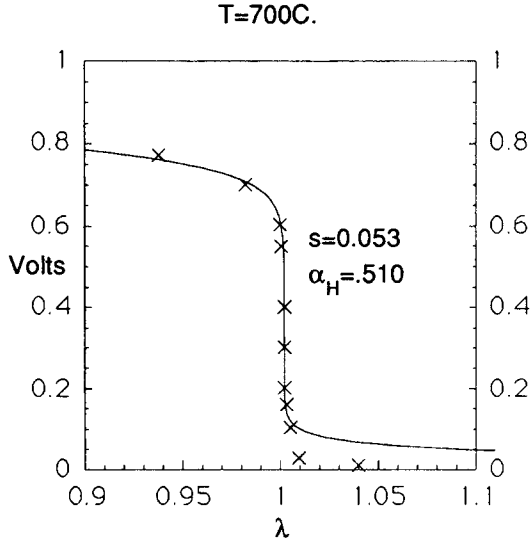

Figure 8. Comparison of the model fit with the experimental data (Logothetis, 1981).

Fit values for α_H and $s = s_I = s_{II}$ are shown.

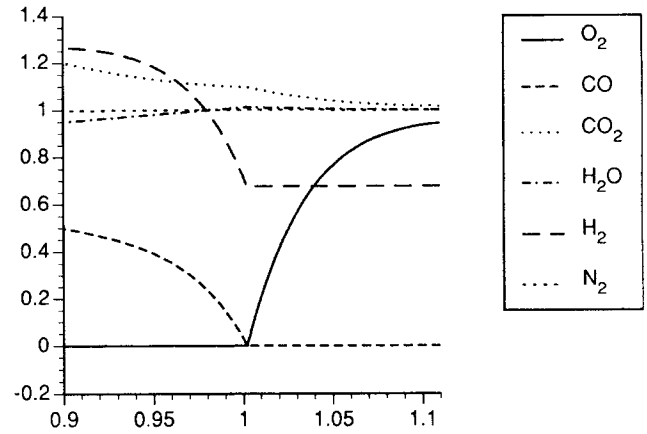

Figure 9. Surface concentrations (x_i/x_i^∞) vs. engine equivalence ratio (λ).

in Figure 9 for $0.9 \le \lambda \le 1.1$. The dominant gas species (nitrogen, carbon dioxide, and water) tend to maintain rather uniform surface concentrations throughout the range of study. In contrast, the surface concentration of oxygen is nearly zero for rich-gas streams ($\lambda < 1$) and tends toward its bulk-gas-concentration value as the exhaust gas becomes more lean. As expected, the opposite behavior is observed for the carbon monoxide. Since the hydrogen adsorption-desorption reaction is hindered, the hydrogen concentration on the lean side tends toward a value at which

$$\tilde{N}_{\ddot{s}5} = \alpha_H x_5,$$

reflecting the fact that the hydrogen surface concentration θ_5 is tending to zero (Eq. 44). On the rich side, the hydrogen gas concentrations actually climb above their bulk values, reflecting the fact that H_2O is being broken down into hydrogen and oxygen. This can also be seen from the depressed concentration of H_2O on the rich side. One can interpret these facts by noting that the constant K_{II} is smaller than K_I, and the CO-oxidation reaction has depressed the oxygen concentrations to the point where the direction of the H_2-oxidation reaction is reversed.

Discussion

A mathematical model has been proposed for the open-circuit exhaust oxygen sensor, taking into account both the effects of transport through the porous layer covering the electrode and the kinetics of various reactions on the electrode surface. The model can be used to predict the voltage response of the sensor as a function of the equivalence ratio λ, and the model equations have been analyzed to determine how this response depends on various kinetic parameters, as well as on other parameters such as exhaust-gas composition. In particular, we note the following.

When reactions 2–6 are assumed to be in equilibrium and tabulated equilibrium constants for the oxidation reactions are used in the model, the predicted voltage response on the rich side is too high, and the switching point at which the voltage jump takes place is too far into the lean range to be consistent with experimental data.

We found two possible mechanisms for lowering the rich-side voltages to make them consistent with experimental data:

1. modify the two tabulated equilibrium constants $\tilde{K}_{\mathrm{I}}$ and $\tilde{K}_{\mathrm{II}}$ to account for surface adsorption-desorption equilibria, or

2. introduce kinetic hindrance into the oxidation reactions (Eqs. 5 and 6).

The second option would imply that the rich-side voltages vary with the thickness of the porous covering layer; as we are unaware of data supporting this conclusion, we have incorporated the first option into the model. New experimental data could be used to clarify this issue.

We are unable to introduce corrections to the switching point λ_0 without introducing kinetic hindrance into either the oxidation reactions or the adsorption-desorption reactions.

1. When rate constants are introduced into the oxidation reactions (case 3), the general form of the voltage response is shown in Figure 6. The model predicts that two switching points will occur, instead of only one. The largest rate constant determines the size of the rich-side plateau, and the smaller rate constant determines the size of the middle plateau. (See the analysis in Appendix 2.) *The choice of these constants does not, however, influence the location of the switching points.* It should also be noted that when both rate constants are approximately the same size, the middle and the left-most plateaus are equal and only the right-most switching point is observed. As noted above, these rate constants can then be used to vary the rich-side plateau. We know of no data supporting the notion of two switching points and have thus assumed that the two oxidation reactions are in equilibrium.

2. Arguments based on published data cited in the Results section lead us to the conjecture that both the oxygen and the carbon-monoxide adsorption-desorption reactions are in equilibrium, but that hydrogen adsorption-desorption might be hindered. (See case 2 and the discussion in the Results section.) The rate constant for this reaction then appears in a dimensionless parameter α_{H}, which influences the location of the switching point, as shown in Figure 7. Using a Fick's law approximation to the transport in the porous layer, we are able to give a formula (Eq. 45) which determines the location of the switching point. An analogous calculation can be done numerically using the more precise Stefan-Maxwell transport equations. These calculations predict that the switching point should depend on the thickness of the porous layer, and it should be possible to perform experiments to check these predictions.

The assumption of hindered hydrogen adsorption-desorption can be used to calculate the size of the lean shift associated with methanol fuel mixtures, if the associated gas concentrations x_i^e are known for the fuel mixtures under consideration. In such calculations, one would fit the parameters α_{H} and s to the data from one fuel mixture (say gasoline) and then use the same parameter values to do calculations with gas concentrations from the methanol mixture. The resulting lean shift can also be more simply approximated using formula 45, used for calculating the switching point assuming transport given by Fick's law, and some important aspects of this phenomenon can be understood by examining this equation. In particular, note that each gas concentration in Eq. 45 appears multiplied by its diffusion coefficient $D_{i6}x_i^e$. If all diffusion coefficients were equal and hydrogen adsorption were equilibrated ($\alpha_{\mathrm{H}}=\infty$), then the switching point would occur at stoichiometry. The fact that the diffusion coefficient D_{56} for hydrogen in nitrogen is about 4 times the size of other diffusion coefficients displaces the switching point in the lean direction. Formula 45 predicts, however, that by decreasing α_{H}, for example, by decreasing the porous coating thickness L, it is possible to move the switching point back toward the stoichiometric point. It should be possible to perform experiments to check these predictions.

Notation

c = total concentration, mol/cm^3
D_{ij} = diffusion coefficient for species i relative to species j, cm^2/s
F = Faraday's constant, 96,487 C/equivalent
k = rate constant
$K, \tilde{K}$ = equilibrium constants
L = thickness of the porous layer, cm
n = unit normal vector pointing into the porous layer
N_{zi} = flux value for species i, mol/cm$^2\cdot$s
p = pressure, atm
$p_{1,\mathrm{ref}}$ = oxygen partial pressure in the reference chamber, atm
R = gas constant, 8.314 J/mol$\cdot$K
s = scale factor for equilibrium constants
T = temperature, K
V = electrode potential, V
x = mole fraction
z = distance from the electrode in the porous layer, cm

Greek letters

α_{H} = dimensionless rate constant for hydrogen adsorption
ϵ = $1/K_{\mathrm{I}}\sqrt{p}$
λ = equivalence ratio, Eq. 1
λ_0 = value of the equivalence ratio at the switching point
Θ_i = θ_i/θ_v
τ = tortuosity factor

Subscripts

b, i = backwards rate constant for species i
f, i = forward rate constant for species i
i = species i
v = fractional surface coverage of vacant sites

Superscripts

e = well-mixed concentration-values in exhaust outside the porous layer
$\tilde{}$ = dimensionless parameter

Literature Cited

Anderson, J. E., and Y. B. Graves, "Steady-State Characteristics of Oxygen Concentration Cell Sensors Subjected to Nonequilibrium Gas Mixtures," *J. Electrochem. Soc.*, **128**, 294 (1981).

Asad, A. M., S. A. Akbar, S. G. Mhaisalkar, L. D. Birkefeld, and K. S. Goto, "Solid-State Gas Sensors: A Review," *J. Electrochem. Soc.*, **139**, 3690 (1992).

Baker, D. R., "Reducing Nonlinear Systems of Transport Equations to Laplace's Equation," *SIAM J. of Appl. Math.*, **53**(2), 419 (1993).

Berlowitz, P. J., C. H. F. Peden, and D. W. Goodman, "Kinetics of CO Oxidation on Single-Crystal Pd, Pt, Ir," *J. Phys. Chem.*, **92**, 5213 (1988).

Bird, R. B., W. E. Stewart, and E. N. Lightfoot, *Transport Phenomena*, Wiley, New York (1960).

Bonzel, H. P., and J. J. Burton, "CO Oxidation on a Pt(110) Surface: Solution of Reaction Model," *Surf. Sci.*, **52**, 223 (1975).

Bonzel, H. P., and R. Ku, "Mechanisms of the Catalytic Carbon Monoxide Oxidation on Pt(110)," *Surf. Sci.*, **33**, 33 (1972a).

Bonzel, H. P., and R. Ku, "Carbon Monoxide Oxidation on a Pt(110) Single Crystal Surface," *J. Vac. Sci. and Tech.*, **9**, 663 (1972b).

Brailsford, A. D., and E. M. Logothetis, "A Steady-State Diffusion Model for Solid-State Gas Sensors," *Sensors and Actuators*, **7**, 39 (1985).
Dietz, H., W. Haecker, and H. Jahnke, "Electrochemical Sensors for the Analysis of Gases," *Advances in Electrochemistry and Electrochemical Engineering*, Vol. 10, H. Gerischer and C. W. Tobias, eds., Wiley, New York (1977).
Eddy, D. S., "Electrochemical Apparatus for Monitoring Exhaust Gases," U. S. Patent 3616274 (Oct. 26, 1971).
Engel, T., and G. Ertl, "Elementary Steps in the Catalytic Oxidation of Carbon Monoxide on Platinum Metals," *Advances in Catalysis*, D. D. Eley, H. Pines, and P. B. Weisz, eds., Vol. 28, p. 1 (1979).
Epstein, N., "On Tortuosity and the Tortuosity Factor in Flow and Diffusion through Porous Media," *Chem. Eng. Sci.*, **44**, 777 (1989).
Etsell, T. H., and S. N. Flengas, "The Electrical Properties of Solid Oxide Electrolytes," *Chem. Rev.*, **70**, 339 (1970).
Fleming, W. J., "Zirconia Oxygen Sensor—An Equivalent Circuit Model," SAE 800020 (1981).
Flemming, W. J., D. Howarth, and D. S. Eddy, "Sensor for On-Vehicle Detection of Engine Exhaust Gas Composition," SAE 730575 (1973).
Fouletier, J, P. Fabry, and Kleitz, "Electrochemical Semipermeability and the Electrode Microsystem in Solid Oxide Electrolyte Cells," *J. Electrochem. Soc.*, **123**, 204 (1976).
Haaland, D. M., "Noncatalytic Electrodes for Solid-Electrolyte Oxygen Sensors," *J. Electrochem. Soc.*, **127**, 796 (1980).
Heyne, L., "Some Properties and Applications of Zirconia-Based Solid-Electrolyte Cells," *Measurement of Oxygen*, H. Degn, I. Balslev, and R. Brook, eds., Elsevier, Amsterdam (1976).
Heyne, L., "Ionic Conductivity in Oxides," *Mass Transport in Oxides*, J. B. Wachtman, Jr. and A. D. Franklin, eds., Nat. Bur. of Standards, Special Publication 296, p. 149 (1968).
Heyne, L., and D. den Engelsen, "The Speed of Response of Solid Electrolyte Galvanic Cells for Gas Sensing," *J. Electrochem. Soc.*, **124**, 727 (1977).
Hirschfelder, J. O., C. F. Curtiss, and R. B. Bird, *Molecular Theory of Gases and Liquids*, Wiley, New York, p. 718 (1954).
Hori, G. K., and L. D. Schmidt, "Transient Kinetics in CO Oxidation on Platinum," *J. Catal.*, **38**, 335 (1975).
Kröger, F. A., and H. J. Vink, "Relations between the Concentrations of Imperfections in Crystalline Solids," *Solid State Physics—Advances in Research and Applications*, Vol. 3, Academic Press, New York, p. 307 (1956).
Laidler, K. J., *Chemical Kinetics*, 2nd ed., McGraw-Hill, New York (1965).
Langmuir, I., "The Mechanism of the Catalytic Action of Platinum in the Reactions $2CO+O_2=2CO_2$ and $2H_2+O_2=2H_2O$," *Trans. Farad. Soc.*, **17**, 621 (1921-1922).
Logothetis, E. M., "ZrO_2 Oxygen Sensors in Automotive Applications," *Science and Technology of Zirconia II*, A. H. Heuer and L. W. Hobbs, eds., *Amer. Chem. Soc.*, Columbus, OH (1981).
Maskell, W. C., and B. C. H. Steele, "Solid State Potentiometric Oxygen Gas Sensors," *J. Appl. Electrochem.*, **16**, 475 (1986).
Matsushima, T., D. B. Almy, and J. M. White, "The Reactivity and Auger Chemical Shift of Oxygen Adsorbed on Platinum," *Surf. Sci.*, **67**, 89 (1977).
Mizusaki, J., K. Amano, S. Yamauchi, and K. Fueki, "Electrode Reaction at $Pt,O_2(g)$/Stabilized Zirconia Interfaces: I. Theoretical Consideration of Reaction Model," *Solid State Ionics*, **22**, 313 (1987a).
Mizusaki, J., K. Amano, S. Yamauchi, and K. Fueki, "Electrode Reaction at $Pt,O_2(g)$/Stabilized Zirconia Interfaces: II. Electrochemical Measurements and Analysis," *Solid State Ionics*, **22**, 323 (1987b).
Mizusaki, J., J. Tagawa, Y. Miyaki, S. Yamauchi, K. Fueki, I. Koshiro, and K. Hirano, "Kinetics of the Electrode Reaction at the $CO-CO_2$ Porous Pt/Stabilized Zirconia Interface," *Solid State Ionics*, **53-56**, 126 (1992).
Okamoto, H., G. Kawamura, and T. Kudo, "Relation between Surface Adsorption States and emf in a Solid Electrolyte Concentration Cell during Carbon Monoxide Oxidation on Platinum Studied by Local Current Measurement," *J. Catal.*, **86**, 437 (1984).
Pacia, N., A. Cassuto, A. Pentenero, B. Weber, H. P. Bonzel, and R. Ku, "Molecular Beam Study of the Mechanism of Carbon Monoxide Oxidation on Platinum and Isolation of Elementary Steps," *J. Catal.*, **41**, 455 (1976).
Palmer, R. L., and J. N. Smith, Jr., "Molecular Beam Study of CO Oxidation on a (111) Platinum Surface," *J. Chem. Phys.*, **60**, 1453 (1974).
Patterson, J. W., E. C. Bogren, and R. A. Rapp, "Mixed Conduction in $Zr_{0.85}Ca_{0.15}O_{1.85}$ and $Th_{0.85}Y_{0.15}O_{1.925}$ Solid Electrolytes," *J. Electrochem. Soc.*, **114**, 752 (1967).
Robertson, N. L., and J. N. Michaels, "Oxygen Exchange on Platinum Electrodes in Zirconia Cells: Location of Electrochemical Reaction Sites," *J. Electrochem. Soc.*, **137**, 129 (1990).
Sasayama, T., T. Yamauchi, R. Byers, S. Suzuki, and S. Ueno, "Air-Fuel Ratio Sensor Utilizing Ion Transportation in Zirconia Electrolyte," SAE 910501 (1991).
Smith, J. M., and H. C. Van Ness, *Introduction to Chemical Engineering Thermodynamics*, 3rd ed., p. 390, McGraw-Hill, New York (1975).
Trapnell, B. M. W., *Chemisorption*, Butterworths Scientific Publications, London (1955).
Verbrugge, M. W., and D. W. Dees, "Theoretical Analysis of a Blocking-Electrode Oxygen Sensor for Combustion-Gas Streams," *J. Electrochem. Soc.*, **140**, 2001 (1993).
Wagner, C., "Equations for Transport in Solid Oxides and Sulfides of Transition Metals," *Progress in Solid-State Chemistry*, Vol. 10, Pergamon Press, Great Britain, p. 3 (1975).
Young, C. T., and J. D. Bode, "Characteristics of ZrO_2-Type Oxygen Sensors for Automotive Applications," SAE 790143 (1980).

Appendix 1: Diffusion-Coefficient and Bulk-Concentration Values

The quantities appearing in this section are assumed to be always in their dimensioned form. The relative diffusion coefficients $D_{i,j}$ in this study were calculated from (Bird et al., 1960):

$$D_{i,j} = a_{i,j}\left(\frac{T}{\sqrt{T_{C,i}T_{C,j}}}\right)^{b_{i,j}} \frac{(p_{C,i}p_{C,j})^{1/3}(T_{C,i}T_{C,j})^{5/12}\left(\frac{1}{M_i}+\frac{1}{M_j}\right)^{1/2}}{p}, \tag{A1}$$

where T is temperature in Kelvin and p is pressure in atm. The parameters $a_{i,j}$ and $b_{i,j}$ have the values:

$$a_{i,j} = \begin{cases} 2.745\times10^{-4} & \text{if neither } i \text{ nor } j \text{ equals 4,} \\ 3.640\times10^{-4} & \text{otherwise,} \end{cases}$$

$$b_{i,j} = \begin{cases} 1.823 & \text{if neither } i \text{ nor } j \text{ equals 4,} \\ 2.334 & \text{otherwise.} \end{cases}$$

The other parameters are given in Table A1. Equation A1 results from a combination of kinetic theory and corresponding-states arguments and should be appropriate for the relatively low pressures of this study.

The functions $x_i^e(\lambda)$ were approximated by sixth-degree polynomials fit to published data in Figure 2. Specifically,

$$x_i^e = \sum_{j=0}^{6} c_{ij}\lambda^j, \tag{A2}$$

for $i \le 5$, and

Table A1. Parameter Values for Calculating Diffusion Coefficients $D_{i,j}$

Species i	M_i	$T_{C,i}$(K)	$p_{C,i}$(atm)
1	32.00	154.4	49.7
2	28.01	133	34.5
3	44.01	304.2	72.9
4	18.02	647.3	218.3
5	2.016	33.3	12.8
6	28.02	126.2	33.5

$$x_6^e = 1 - \sum_{i=1}^{5} x_i^e.$$

Values for the coefficients c_{ij} are given in Table A2 and

$$y = \frac{2(\lambda - \lambda_1) - 1.9617}{0.6103}. \tag{A3}$$

It was originally intended to use formulas A2 and A3 with $\lambda_1 = 0$, in which case $-1 \le y \le 1$ as λ ranges over the data values between 0.6757 and 1.286. This formula does not, however, satisfy the stoichiometric condition:

$$x_1^e = \frac{x_2^e + x_5^e}{2} \tag{A4}$$

at $\lambda = 1$, and a small correction λ_1 was added to rectify this situation. The parameter λ_1 was numerically determined to be -0.00444829.

Appendix 2: Analysis of Nonequilibrium Situation for Oxidation Reactions

We analyze here the equation system 12-15 (with the fluxes in dimensionless form), Eqs. 46 and 47 arising when the two oxidation reactions 5 and 6 are not in equilibrium. The generic form of the λ-voltage curves in such situations contains two voltage jumps, instead of the single jump appearing in the other model situations so far examined.

The analysis can be based either on the Stefan-Maxwell transport law or Fick's law; we will use Fick's law because it simplifies somewhat the exposition. All variables in this appendix are assumed to be in scaled form, and we will simplify the notation by dropping the ˜ that appeared earlier.

Table A2. Coefficients c_{ij} Used in Formula A2

		j			
		0	1	2	3
i	1	0.5844e−02	0.2182e−01	0.4298e−01	0.7257e−02
	2	0.1328e−01	−0.6245e−01	0.9524e−01	−0.4259e−02
	3,4	0.1387e+00	0.2866e−01	−0.9938e−01	−0.3886e−01
	5	0.4427e−02	−0.2082e−01	0.3175e−01	−0.1397e−02

		j		
		4	5	6
i	1	−0.4051e−01	−0.5163e−02	0.1833e−01
	2	−0.6559e−01	0.2759e−02	0.2314e−01
	3,4	0.1266e+00	0.2862e−01	−0.7155e−01
	5	−0.2191e−01	0.9022e−03	0.7744e−02

It will be convenient to rewrite Eqs. 46 and 47 in the form:

$$\epsilon_3 N_{z3} = -x_2\sqrt{x_1} + \epsilon_0 x_3 \tag{A5}$$

$$\epsilon_4 N_{z4} = -x_5\sqrt{x_1} + \epsilon_0 K x_4, \tag{A6}$$

where $\epsilon_i = 1/k_i$ for $i = 3, 4$; as a notational convenience, we relabel the parameter ϵ by giving it a subscript 0. We will start the analysis by considering the case in which

$$\epsilon_0 \ll \epsilon_3 \ll \epsilon_4 \ll 1. \tag{A7}$$

Once this has been done, it should be clear how to generalize the analysis to situations in which ϵ_i satisfy inequalities different from the above. When Eq. A7 holds, the two switching points will be the boundaries for three different regions of the equivalence ratio λ. These are the regions in which

(i) $x_1(1)$ is $O(1)$, $x_2(1)$ is $O(\epsilon_3)$, and $x_5(1)$ is $O(\epsilon_4)$,
(ii) $x_1(1)$ is $O(\epsilon_4^2)$, $x_2(1)$ is $O(\epsilon_3/\epsilon_4)$, and $x_5(1)$ is $O(1)$,
(iii) $x_1(1)$ is $O(\epsilon_3^2)$, $x_2(1)$ is $O(1)$, and N_{z4} is $O(\epsilon_3/\epsilon_4)$.

We will refer λ_0 as the boundary between regions (i) and (ii), and λ_1 as the boundary between regions (ii) and (iii). Figure 6 shows an example of a typical λ-voltage curve for such a situation, with the boundaries λ_0 and λ_1, as well as the voltage behavior in each region.

To do the calculations in region (i), we assume that x_i can be written as multivariable Taylor series in the variables ϵ_i. By assumption, ϵ_0 is much smaller than the other two ϵ_i, so that terms of order ϵ_0 in Eqs. A5 and A6 will drop out of the leading order analysis and can thus be ignored in the Taylor expansion. To leading order we write:

$$x_i(z) = x_{i,0,0}(z) + \epsilon_3 x_{i,1,0}(z) + \epsilon_4 x_{i,0,1}(z) + \ldots \tag{A8}$$

If $x_{1,0,0}(1)$ is nonzero, it follows from Eqs. A5 and A6 that:

$$x_{2,0,0}(1) = x_{5,0,0}(1) = 0,$$

and these two equations with the four flux equations (Eqs. 12-15) can be used to solve for the terms $N_{zi,0,0}$ and $x_{i,0,0}$. The term $x_{1,0,0}(1)$ can now be used in Eq. 29 to calculate the voltage to leading order.

To do the calculations in region (ii), we assume that x_i can be written as multivariable Taylor series in the variables ϵ_0, ϵ_3/ϵ_4, and ϵ_4. Again, ϵ_0 terms can be ignored in the leading-order analysis, and we use the same subscripting conventions as in case (i), except that the first subscript now designates powers in ϵ_3/ϵ_4. If $x_{5,0,0}(1)$ is nonzero, it follows from Eqs. A5 and A6 that $x_{1,0,2}(1)$ is the first nonvanishing term for x_1 and, since $\epsilon_3 \ll \epsilon_4$, $x_{2,1,0}(1)$ must be the first nonvanishing term for x_2. To calculate the terms $N_{zi,0,0}(1)$, one thus uses the four flux equations (Eqs. 12-15) and the two equations:

$$x_{1,0,0}(1) = x_{2,0,0}(1) = 0.$$

Equation A6 then implies that:

$$N_{z4,0,0}(1) = -x_{5,0,0}(1)\sqrt{x_{1,0,2}(1)},$$

which can be used to calculate $x_{1,0,2}(1)$. The leading order expression for $x_1(1)$, which must be inserted into Eq. 29 to calculate the voltage, is then $\epsilon_4^2 x_{1,0,2}(1)$.

To do the calculations in region (iii), we assume that x_i can be written as multivariable Taylor series in the variables ϵ_0, ϵ_3, and ϵ_3/ϵ_4, and use the same subscript conventions as in case (i), except that the second subscript now designates powers in ϵ_3/ϵ_4. If $x_{2,0,0}(1)$ is nonzero, it now follows that $x_{1,2,0}(1)$ is the first nonvanishing term for x_1 and, since $N_{z4} = -N_{z5}$, $N_{z5,0,1}$ is the first nonvanishing term for N_{z5}. From Fick's law, it now follows that:

$$x_{5,0,0}(1) = x_5^e \quad \text{and} \quad x_{1,0,0}(1) = 0.$$

To calculate the terms $x_{i,0,0}(1)$ one thus uses the above two equations, as well as the four flux equations (Eqs. 12–15). Equation A5 then implies that:

$$N_{z3,0,0}(1) = -x_{2,0,0}(1)\sqrt{x_{1,2,0}(1)},$$

which can be used to calculate the leading order expression $\epsilon_3^2 x_{1,2,0}(1)$ for $x_1(1)$. This expression is then used in Eq. 29 to calculate the voltage.

At the boundary λ_0 between regions (i) and (ii), the following equations must hold:

$$x_{1,0,0}(1) = x_{2,0,0}(1) = x_{5,0,0}(1) = 0.$$

These are the same as equations used to find the switching point when all reactions are in equilibrium, and it follows that λ_0 will be this switching point determined by Eq. 43. At the boundary λ_1 between regions (ii) and (iii), the following conditions must hold:

$$x_{1,0,0}(1) = x_{2,0,0}(1) = -N_{z5,0,0} = 0.$$

These equations also determine the switching point when the hydrogen reaction is turned off, and it follows that λ_1 will be this switching point, determined by the equation:

$$D_{16} x_1^e = \frac{D_{26} x_2^e}{2}.$$

The middle region (ii) thus serves as a transition between the plateaus on the rich and lean sides. As ϵ_4 varies, clearly the value of this middle region will shift up and down. In particular, if ϵ_3 and ϵ_4 are of the same order, then the middle region will be at the same level as the rich-side region (iii). The switching point λ_1 will thus vanish, and the only voltage switch that will be apparent will be λ_0. If ϵ_3 and ϵ_4 are of the same order, but ϵ_3 is varied, it also follows that the rich-side plateau will also vary, as was noted in the Results section. Because the dimensionless parameters $\epsilon_i = 1/k_i$ depend on the effective pore length L, this would then imply that the rich-side plateau also depends on L.

As ϵ_4 is increased, the middle plateau will rise until, when ϵ_4 becomes $O(1)$, the middle plateau is at the same height as the lean-side plateau in region (i). In this case, one will again see only one switching point, namely λ_1, and the switching occurs as if the hydrogen reaction were turned off. Finally, we note that if both ϵ_3 and ϵ_4 are increased until they become $O(1)$, the plateaus in both regions (ii) and (iii) will rise until they are at the same level as the lean-side plateau in region (i). In this case, one would see no switching points at all.

Appendix 3: Singular Perturbation Analysis Near the Switching Point

As noted earlier, the perturbation analysis becomes invalid when the bulk concentration values x_i^e are close to the values at which the jump between the different solution branches to Eq. 38 takes place. In this appendix, we give a different expansion in powers of $\epsilon^{2/3}$, which is valid near this switching point, and we show that the two expansions agree with each other at λ values far enough from the switching point. Although we will give the analysis here using the assumption that all reactions are in equilibrium, this analysis can be extended to the more general situation in a straightforward manner. All variables in this appendix are scaled, and to simplify the notation we will drop the ~ over these variables in the following exposition.

As in Appendix 2, we restrict our attention here to the case where transport is governed by Fick's law. The analysis using the Stefan-Maxwell equations can be handled in a similar manner.

The perturbation analysis away from the switching point was made under the assumption that the value of λ is to remain constant while ϵ varies; the analysis given here will not make this assumption. Specifically, we define:

$$\bar{\lambda} = \epsilon^{-2/3}(\lambda - \lambda_0),$$

where λ_0 is the switching point determined by Eq. 43, and it will be assumed that $\bar{\lambda}$ remains constant as ϵ is varied. This means, in particular, that λ tends to λ_0 as ϵ tends to zero. We will use a superscript zero to denote the value of any variable in the leading order expansion in ϵ; for example, $x_i^{e,0} = x_i^e(\lambda_0)$ are the bulk concentration values satisfying Eq. 43, N_{zi}^0 are the associated leading-order fluxes, and $x_i^0(1)$ are the leading order concentrations. Define

$$\bar{x}_i^e = \epsilon^{-2/3}[x^e(\lambda) - x^{e,0}].$$

We postulate then that

$$N_{z_i} = N_{z_i}^0 + \epsilon^{2/3}\bar{N}_{z_i} + \ldots \tag{A9}$$

$$x_i = x_i^0 + \epsilon^{2/3}\bar{x}_i + \ldots, \tag{A10}$$

where the terms not written are assumed to be at least of order $\epsilon^{4/3}$, and $\bar{N}_{zi}$ and $\bar{x}_i$ are functions of $\bar{\lambda}$, and hence independent of ϵ during the perturbation. Note that we can also write:

$$\bar{x}_i^e = \bar{\lambda}\frac{dx_i^e}{d\lambda}(\lambda_0) + \ldots, \tag{A11}$$

where the terms not written are at least of order $\epsilon^{2/3}$.

Equation 34 and the fact that $x_1^0(1) = x_2^0(1) = 0$, now imply that:

$$x_3^0(1) = \bar{x}_2(1)\sqrt{\bar{x}_1(1)}, \tag{A12}$$

and Eq. 40, along with the fact that $x_3^0(1)=0$, implies that:

$$\tilde{K}x_4^0(1)\bar{x}_2(1)=x_3^0(1)\bar{x}_5(1). \tag{A13}$$

Equations A12-A13, along with the flux equations (Eqs. 12-15) can be used to solve for $\bar{N}_{z1}, \ldots, \bar{N}_{z6}$ so that $\bar{N}_{z1}$ can then be used in Fick's law to calculate $\bar{x}_1(1)$. The leading-order expression

$$x_1(1)=\epsilon^{2/3}\bar{x}_1(1)+\ldots$$

can now be used in Eq. 29 to calculate the voltage when

$$\lambda=\lambda_0+\epsilon^{2/3}\bar{\lambda}.$$

The resulting six equations for the unknown fluxes were simplified, using a symbolic manipulation package, leading to the equation:

$$\frac{(D_{1,6}\bar{x}_1^e-\bar{N}_{z1})\,(D_{2,6}\bar{x}_2^e+D_{5,6}\bar{x}_5^e-2\bar{N}_{z1})^2}{D_{1,6}[D_{2,6}x_3^0(1)+D_{5,6}\tilde{K}x_4^0(1)]^2}=1.$$

This is a cubic polynomial in $\bar{N}_{z1}$ which must be solved to calculate $\bar{x}_1$ using Fick's law.

To compare this solution with the one developed earlier, recall that, as ϵ goes to zero and λ is held fixed, $\bar{\lambda}$ tends to $\pm\infty$. Thus, one expects that the two expansions should agree with each other in the limit of large $|\bar{\lambda}|$. To verify this it is necessary to rewrite the leading-order solutions as functions of $\bar{\lambda}$ instead of λ and to compare them with the solution $\bar{x}_1$ described above. Recalling that $x_{i,0}$ is the leading order term for x_i using the expansion discussed earlier, it is useful to define the terms $\bar{x}_{i,0}$ by the equation:

$$x_{i,0}=x_i^0+\epsilon^{2/3}\bar{x}_{i,0}+\ldots,$$

where $\bar{x}_{i,0}$ (and the higher-order terms not written) depend on $\bar{\lambda}$ instead of λ, and it follows that:

$$x_{i,0}=\epsilon^{2/3}\bar{x}_{i,0}+\ldots,$$

for $i=1, 2, 5$.

Recalling that $x_{1,0}(1)=0$ when $\lambda<\lambda_0$ and $x_{2,0}(1)=0$ when $\lambda>\lambda_0$, one then shows that:

$$\bar{x}_{1,0}(1)=\bar{x}_1^e-\frac{D_{2,6}\bar{x}_2^e+D_{5,6}\bar{x}_5^e}{2D_{1,6}}$$

when $\lambda>\lambda_0$, and

$$\bar{x}_{1,2}(1)=\left[\frac{x_3^0(1)}{\bar{x}_{2,0}(1)}\right]^2=\left[\frac{D_{2,6}x_3^0(1)+D_{5,6}Kx_4^0(1)}{2D_{1,6}\bar{x}_1^e-D_{2,6}\bar{x}_2^e-D_{5,6}\bar{x}_5^e}\right]^2$$

when $\lambda<\lambda_0$. The quantity $\bar{x}_{1,0}(1)$ should then tend to $\bar{x}_1$ in the limit as $\bar{\lambda}\to\infty$ and $\bar{x}_{1,2}(1)$ should then tend to $\bar{x}_1$ in the limit as $\bar{\lambda}\to-\infty$.

Figure 4 shows a comparison of the natural logs of the leading-order terms $\bar{x}_{1,0}(1)$ and $\bar{x}_{1,2}(1)$ (associated with the perturbation series away from the switching point with the natural log of the leading-order term $\bar{x}_1(1)$ (given in this appendix). Each of these terms is plotted as a function of $\bar{\lambda}$. The plot was made by assuming a temperature of 973 K to derive values for the diffusion coefficients (as described in Appendix 1) and the equilibrium constants K_i as described in the main text. Although some of the diffusion coefficients and the parameter $\tilde{K}$ are temperature-dependent, they are considered to be quantities independent of ϵ for these calculations, and their variations over the temperature range considered here should not significantly alter the qualitative picture given in Figure 4. The value $\lambda_0=1.01352$ was found by numerically solving Eq. 43 using the functions $x^e(\lambda)$ (Appendix 1), and the functions $\bar{x}^e(\bar{\lambda})$ were evaluated using the first-order approximations in Eq. A11. The plot shows that the expansions in the main text agree well with the expansion in this appendix, when $\bar{\lambda}<-10$ or $\bar{\lambda}>20$. As noted earlier, the parameter ϵ at these temperatures is on the order of 10^{-10}, so that the region of λ values for which the approximations become inaccurate has a width on the order of 7×10^{-6}.

Appendix 4: Boundary Conditions When θ_v Is Allowed to Vary

The boundary conditions (Eqs. 18-22) are based on the assumption that the fractional coverage θ_v of vacant sites is constant. Without this assumption, these equations take the form:

$$N_{z1}/\theta_v^2=k_{f,1}x_1-k_{b,1}(\theta_1/\theta_v)^2 \tag{A14}$$

$$N_{z2}/\theta_v=k_{f,2}x_2-k_{b,2}\theta_2/\theta_v \tag{A15}$$

$$N_{z5}/\theta_v^2=k_{f,5}x_5-k_{b,5}(\theta_5/\theta_v)^2 \tag{A16}$$

$$N_{z3}/\theta_v^2=k_{f,3}x_3-k_{b,3}\theta_2\theta_1/\theta_v^2 \tag{A17}$$

$$N_{z4}/\theta_v^3=k_{f,4}x_4-k_{b,4}\theta_5^2\theta_1/\theta_v^3. \tag{A18}$$

Equations 18-22 were obtained by clearing fractions and lumping the appropriate powers of θ_v (assumed constant) in with the corresponding rate constants.

We will show that it is possible to do model calculations without the assumption that θ_v is constant, although the resulting model is more complicated than the one that assumes constant θ_v. We will also present arguments to show that many of the model results derived by assuming constant θ_v still remain valid without this assumption. The five equations (Eqs. A14-A18) can be used in conjunction with the four flux equations (Eqs. 12-15) to make a total of nine equations in the unknowns $N_{z1}, \ldots, N_{z6}$, and θ_1, θ_2, θ_5. (Recall that the mole fractions x_i are functions of the N_{zi} via Eq. 11 and that θ_v is the difference between 1 and the sum of the other θ_i, see Eq. 17.) We turn now to the analogues of cases 1-3. Key to the discussion will be the assertion that the quantity $1/\theta_v$ never becomes extremely large, which amounts to the assertion that the fractional coverage θ_v of vacant sites never becomes too small.

Case 1: Equilibrated Interface. If the lefthand sides of Eqs. A14-A18 are much smaller than each of the summands on the right, then reactions 2-6 can be modeled as equilibrated. (Note that the size of θ_v affects when equilibrium conditions will hold.) Under the equilibrium assumption, the lefthand sides of these equations are set to zero, and the analysis pro-

ceeds in the same way as discussed in the main text. Variations in θ_v then make no difference in the resulting model equations.

Case 2: Hindered Hydrogen Adsorption-Desorption. Equations A14–A15 are in equilibrium form, but Eq. A16 is not. From Eq. A16 and arguments similar to those given for case 2, one obtains the equation:

$$\frac{x_4}{\left(x_5 - \frac{N_{z5}}{\theta_v^2 k_{f,5}}\right)\sqrt{x_1}} = K_{II}\sqrt{p}, \tag{A19}$$

which is the analogue to Eq. 26. Variations in θ_v will presumably change the shape of the voltage-response curve and could also influence the position of the switching point, if the factor θ_v in Eq. A19 is significantly different from 1. This factor would then change the value of α_H that was fit to the data. To determine x_1 (and thus the voltage) away from the switching point, it is necessary to solve for the θ_i/θ_v in terms of the x_i. To do this, one uses the equilibrium forms of Eqs. A14 and A15 to write:

$$(\theta_1/\theta_v)^2 = \frac{k_{f,1}}{k_{b,1}}\, x_1$$

$$\theta_2/\theta_v = \frac{k_{f,2}}{k_{b,2}}\, x_2,$$

and these equations and Eq. A19 determine θ_1, θ_2, and θ_v, from which θ_5 can also be determined. This necessitates the introduction of two new parameters into the equations ($k_{f,i}/k_{b,i}$ for $i = 1, 2$).

Case 3: Equilibrium Adsorption-Desorption, Hindered Oxidation. In this case, Eqs. 27 and 28 become:

$$N_{z3}/\theta_v^2 = k_3\left(-x_2\sqrt{x_1} + \frac{x_3}{K_I\sqrt{p}}\right)$$

$$N_{z4}/\theta_v^3 = k_4\left(-x_5\sqrt{x_1} + \frac{x_4}{K_{II}\sqrt{p}}\right).$$

The two switching points determined as in Appendix 2 are given (to leading order) by:

$$x_1 = x_2 = x_5 = 0$$

for the lean-side switching point and

$$x_1 = x_2 = N_{z4}/\theta_v^3 = 0$$

for the rich-side switching point. Because $1/\theta_v$ is always greater than one, N_{z4} must equal zero at the rich-side switching point, and these equations determine the same switching points in Appendix 2.

Manuscript received June 16, 1993, and revision received Oct. 15, 1993.